for these objects[18], our data place an upper limit of 1.2×10^{-3} pc^{-3} for zero-metallicity stars of this mass in a uniform halo, that is, a limit more stringent than the upper limits derived above for stars of disk or halo metallicity.

Because our conclusions are based on four spatially separate fields, they should prove an unbiased sampling of the halo, free from biases due to clumping or other structure. Our number-density limits eliminate any possibility that stars at or near the hydrogen-burning limit contribute any significant fraction of the dynamical mass of the halo, irrespective of metallicity.

Turning again to the $(I-K')>6$ data, we have compared the absence of such objects with the expectation based on the K-band luminosity function derived by Nelson *et al.*[19] under the assumption of constant star formation rates but with a variety of mass functions (IMFs). Adopting their $T_{max} = 1{,}500$ K curves, where T_{max} is the maximum effective temperature of stars contributing to the luminosity function, as very roughly corresponding to an $(I-K')>6$ colour selection we find that, scaling their standard model to the field galactic latitudes (typically around 45°), the expected number of $(I-K')>6$ stars integrated to $K' = 19$ mag is $1.2 \times (\rho/(0.10 M_{\odot}\ \mathrm{pc}^{-3}))$, where ρ is the local density associated with dark matter, and is relatively insensitive to the functional form of the IMF or the choice of T_{max}. The current sample therefore places a 1σ upper limit of $0.08\ M_{\odot}\ \mathrm{pc}^{-3}$ on the local brown-dwarf mass density under the Nelson *et al.*[19] assumptions. Further searches of larger areas are clearly needed to refine this result, and are currently being carried out by one of us (J.-S.H.).

We conclude that little of the halo dark mass can be in hydrogen-burning stars with masses $\gtrsim 0.1 M_{\odot}$ even if these objects are of low metallicity[17]. It appears unlikely that any stellar remnant population can be present in sufficient numbers to account for a significant fraction of the local mass density without violating other astrophysical constraints, and in any case no mechanism to create stellar remnants of such low mass is known. Thus, unless the possible MACHO events (of refs 3 and 4) are attributable to some exotic (and possibly hitherto unknown) objects which are not composed of baryonic matter in its normal state as hydrogen and helium, and so do not become luminous stars, identification of these occurrences, if indeed due to gravitational lensing, is most likely to be with brown dwarfs below the hydrogen-burning limit of $0.07 M_{\odot}$. This mass limit is the approximate limit of current observational extrapolations, as well as a natural fiducial break in physical processes describing the stellar mass function. This explanation has a clear prediction: if the MACHO events are real and caused by compact substellar masses of ordinary baryonic matter, then we predict that as the experiments progress they will see many events of shorter average duration than was seen in the initial detection[3,4]. Very recently, Sahu[20] suggested that the MACHO events may have resulted from lensing by stars in the Large Magellanic Cloud, rather than objects in the halo of our Galaxy. This is consistent with our own conclusions, in that we see no evidence for halo stars of the mass estimated for the MACHO lenses. □

Received 3 November 1993; accepted 24 August 1994.

1. Trimble, V. *A. Rev. Astr. Astrophys.* **25,** 425–472 (1987).
2. Fich, M. & Tremaine, S. *A. Rev. Astr. Astrophys.* **29,** 409–445 (1991).
3. Alcock, C. *et al. Nature* **365,** 621–623 (1993).
4. Aubourg, E. *et al. Nature* **365,** 623–625 (1993).
5. Kroupa, P., Tout, C. A. & Gilmore, G. *Mon. Not. R. astr. Soc.* **262,** 545–587 (1993).
6. Tinney, C. G., Mould, J. R. & Reid, I. N. *Astrophys. J.* **396,** 173–177 (1992).
7. Comeron, F., Rieke, G. H., Burrows, A. & Rieke, M. J. *Astrophys. J.* **416,** 185–203 (1993).
8. Richer, H. B. & Fahlman, G. G. *Nature* **358,** 383–386 (1992).
9. Cowie, L. L. & Songaila, A. *Proc. natn. Acad. Sci. U.S.A.* **90,** 4867–4870 (1993).
10. Songaila, A., Cowie, L. L., Hu, E. M. & Gardner, J. P. *Astrophys. J. Suppl. Ser.* (in the press).
11. Hodapp, K.-W., Rayner, J. & Irwin, E. *Publs. astr. Soc. Pacif.* **104,** 441–451 (1992).
12. Leggett, S. K. *Astrophys. J. Suppl. Ser.* **82,** 351–394 (1992).
13. Hu, E. M. & Ridgway, S. E. *Astr. J.* **107,** 1303–1306 (1994).
14. Becklin, E. E. & Zuckerman, B. *Nature* **336,** 656–658 (1988).
15. Tinney, C. G., Mould, J. R. & Reid, I. N. *Astr. J.* **105,** 1045–1059 (1993).
16. Burrows, A., Hubbard, W. B. & Lunine, J. I. *Astrophys. J.* **345,** 939–959 (1989).
17. Burrows, A., Hubbard, W. B., Saumon, D. & Lunine, J. I. *Astrophys. J.* **406,** 158–171 (1993).
18. Saumon, D., Bergeron, P., Lunine, J. I., Hubbard, W. B. & Burrows, A. *Astrophys. J.* **424,** 333–344 (1994).
19. Nelson, L. A., Rappaport, S. & Joss, P. C. *Astrophys. J.* **404,** 723–733 (1993).
20. Sahu, K. C. *Nature* **370,** 275–276 (1994).
21. Elias, J. H., Frogel, J. A., Matthews, K. & Neugebauer, G. *Astr. J.* **87,** 1029–1034 (1982).
22. Landolt, A. U. *Astr. J.* **104,** 340–371 (1992).
23. Bessell, M. S. & Brett, J. M. *Publs astr. Soc. Pacif.* **100,** 1134–1152 (1988).
24. Bessell, M. S. *Publs. astr. Soc. Pacif.* **102,** 1181–1199 (1990).
25. Bessell, M. S. *Astr. J.* **101,** 662–676 (1991).
26. Wainscoat, R. J. & Cowie, L. L. *Astr. J.* **103,** 332–337 (1992).

A loop-top hard X-ray source in a compact solar flare as evidence for magnetic reconnection

S. Masuda*†, T. Kosugi*, H. Hara*, S. Tsuneta‡ & Y. Ogawara§

* National Astronomical Observatory, Mitaka, Tokyo 181, Japan
‡ Institute of Astronomy, University of Tokyo, Mitaka, Tokyo 181, Japan
§ Institute of Space and Astronautical Science, Sagamihara, Kanagawa 229, Japan

SOLAR flares are thought to be the result of magnetic reconnection—the merging of antiparallel magnetic fields and the consequent release of magnetic energy. Flares are classified into two types[1]: compact and two-ribbon. The two-ribbon flares, which appear as slowly-developing, long-lived large loops, are understood theoretically[2–6] as arising from an eruption of a solar prominence that pulls magnetic field lines upward into the corona. As the field lines form an inverted Y-shaped structure and relax, the reconnection of the field lines takes place. This view has been supported by recent observations[7–10]. A different mechanism seemed to be required, however, to produce the short-lived, impulsive compact flares. Here we report observations made with the Yohkoh[11] Hard X-ray Telescope[12] and Soft X-ray Telescope[13], which show a compact flare with a geometry similar to that of a two-ribbon flare. We identify the reconnection region as the site of particle acceleration, suggesting that the basic physics of the reconnection process (which remains uncertain) may be common to both types of flare.

The flare studied here occurred close to the west limb of the Sun in the active region NOAA 6994 on 13 January 1992 17:25 UT. It was a GOES M2.0-class flare in soft X-rays and showed a single-spike time history in hard X-rays at $\gtrsim 20$ keV. The spike had a duration of ~1 min full-width at half-maximum (FWHM), peaking at 17:28:10 UT. The Hard X-ray Telescope (HXT) and Soft X-ray Telescope (SXT) images are shown in Fig. 1, from which we identify the following essential components. (1) A soft X-ray flaring loop seen in soft X-rays at ~2 keV. We see three bright patches, one at the loop apex and the other two at the ends (footpoints), although the northern footpoint is relatively weak. The intensity variation along the loop, however, is relatively small. The intensity variations along as well as across the loop are mainly due to variations in emission measure $(n_e^2 V)$ where n_e is the number density of electrons and V is the volume, not to variations in electron temperature (T_e). Here, the T_e and $n_e^2 V$ distributions are derived from intensity comparisons between images taken through two different passbands in the 1–2-keV range. The HXT low-energy (14–23 keV) source matches the soft X-ray loop. (2) A high-temperature region above the soft X-ray loop. Electron temperatures are derived to be $\sim 2 \times 10^7$ K. The intensity is weak because of the small emission measure. (3) Double footpoint sources seen in hard X-rays. They

† Present address: Solar Terrestrial Environment Laboratory, Nagoya University, Toyokawa, Aichi 442, Japan.

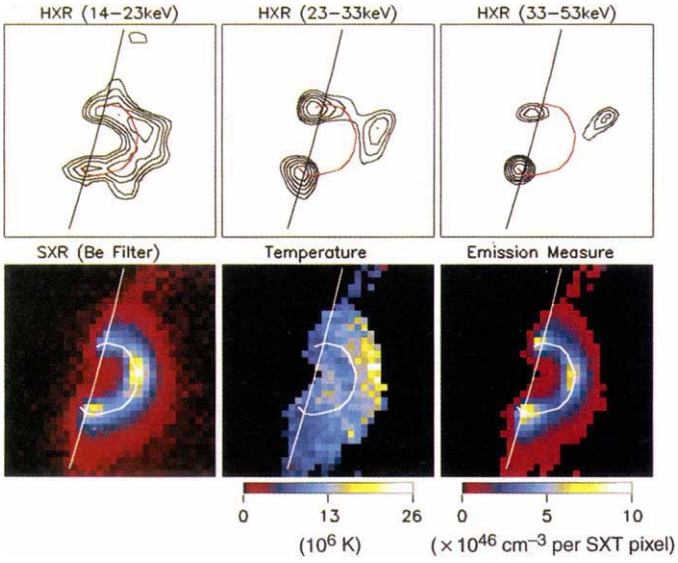

FIG. 1 Hard X-ray (top row) and soft X-ray (bottom row) images of the 13 January 1992 flare that occurred near the west solar limb. HXT images in three HXT energy bands (namely L-, M1-, and M2-bands; 14–23–33–53 keV) are shown at the top for the photon count accumulation interval 17:26:52–17:27:39 UT (rising phase). Contour levels are 70.7, 50.0, 35.4, 25.0 and 17.7% of the peak intensity for each map. At the bottom from left to right are an SXT 119-μm Be-filter image (intensity map) taken at 17:27:01 UT, an electron temperature map, and an emission measure map. The latter two are derived from intensity comparison between the Be-filter image and a 11.6-μm Al-filter image taken at 17:27:07 UT. The field of view of each frame covers 78.4 × 78.4 arcsec or 5.7×10^4 km by 5.7×10^4 km. The SXT pixel size is 2.45 × 2.45 arcsec (~1,800 × 1,800 km). Solar north is to the top, west to the right. For positional reference, the solar limb and the backbone of the soft X-ray flaring loop are shown by solid lines. Accuracy of coalignment is estimated to be within ~1 arcsec.

are dominant at $\gtrsim 25$ keV and located at the footpoints of the soft X-ray loop. The hard X-rays are bremsstrahlung from energetic electrons accelerated near the loop apex and streaming down along the loop toward both ends[14–16]. These sources are also seen in soft X-rays[17,18]. (4) A 'loop-top' hard X-ray source located well above the apex of the soft X-ray loop. Its centroid position is significantly higher than the latter by more than ~10 arcsec or ~7,000 km. (The angular resolutions of SXT and HXT are ~3 and ~5 arcsec respectively.) This source occupies only a small portion of the high-temperature region and has no direct counterpart in the SXT images.

The loop-top hard X-ray source varies rapidly in timescales less than a few tens of seconds and similarly to the footpoint sources (Fig. 2). In addition, judging from the hard X-ray intensities in the different energy bands, the source has a relatively hard spectrum, only slightly softer than those of the footpoint sources. This source only appears for a short interval. Later we see a different class of hard X-ray source near the soft X-ray loop apex which is characterized by a more gradual time variation and a softer spectrum. We call the early hard source a 'loop-top impulsive source' for clarity. Whether this source is of thermal or nonthermal origin is not clear because of lack of detailed hard X-ray spectral information. Because we can perceive a slight spectral softening towards higher energies, it may be interpreted as thermal bremsstrahlung. If this is the case, we get $T_e \sim 2 \times 10^8$ K and $n_e n_i V (\sim n_e^2 V) \sim 5 \times 10^{43}$ cm^{-3}, where n_i is the ion density of the ambient plasma.

The existence of an impulsive hard X-ray source above the soft X-ray flaring loop is of crucial importance. First, it informs us that something energetic is going on outside the bright soft X-ray loop. Second, this something is directly related to particle acceleration. According to Sakao[16], typical double footpoint sources change their intensity simultaneously within a few tenths of a second, which suggests that electrons responsible for the footpoint X-ray emission are accelerated near the loop apex. Taking this into account, it is most likely that we are observing the particle acceleration site directly in the loop-top impulsive source. Finally, the soft and hard X-ray images combined together strongly suggest a magnetic-field geometry with a current sheet in which magnetic reconnection is in progress during the time interval of primary energy release.

The hypothetical scenario depicted in Fig. 3 differs only in detail from standard pictures[19] for two-ribbon flares. For convenience we assume the loop-top impulsive hard X-ray source to be thermal in origin. This corresponds to a maximum value for n_e; if n_i is much larger than n_e the derived value of n_e must be reduced proportionally. Based on the thermal assumption, we get a density $\sim 3 \times 10^8$ cm^{-3}, a total number of electrons (or ions) $\sim 3 \times 10^{35}$, and a thermal energy content $\sim 3 \times 10^{28}$ erg for the hard X-ray emitting 2×10^8-K plasma. (Similarly SXT observations give a density $\sim 2 \times 10^{10}$ cm^{-3} for the 2×10^7-K plasma at the same location. It is not clear, however, whether or not the two components, one seen with HXT and the other with SXT, occupy the same volume.) We speculate that the 2×10^8-K plasma is created as a result of shock heating. This would be possible if the reconnection outflow velocity exceeds ~3,000 km s^{-1}. This velocity is not surprisingly large; an Alfvén velocity of 3,000 km s^{-1} requires a magnetic field intensity of 200 G even when the density is 2×10^{10} cm^{-3}. This intensity is not unreasonable in an active region corona.

The injection rate of electrons (>20 keV) into the footpoint sources, evaluated by adopting the thick target model[20,21], is $\sim 2 \times 10^{35}$ s^{-1} at the peak time (an energy deposition rate of $\sim 1 \times 10^{28}$ erg s^{-1}), using the measured photon power-law index of ~4. This injection rate suggests a high efficiency of acceleration; if we suppose that the electrons stream down from the loop-top source, it means that almost all electrons in the 2×10^8-K plasma would escape in a second or so. Or more probably, the nonthermal electrons are produced directly from the shock in parallel with the creation of the 2×10^8-K plasma. In either case, the reconnection outflow impinging on the loop must have a higher density than that estimated for the 2×10^8-K plasma; from continuity, a density greater than $\sim 2 \times 10^9$ cm^{-3} is required for a shock area $\sim 1 \times 10^{18}$ cm^2 and a shock velocity 3,000 km s^{-1}.

In this scenario, the high-temperature region seen in soft X-rays may be on the periphery of the reconnection outflow, where the outflow velocity is smaller so that only a weak shock

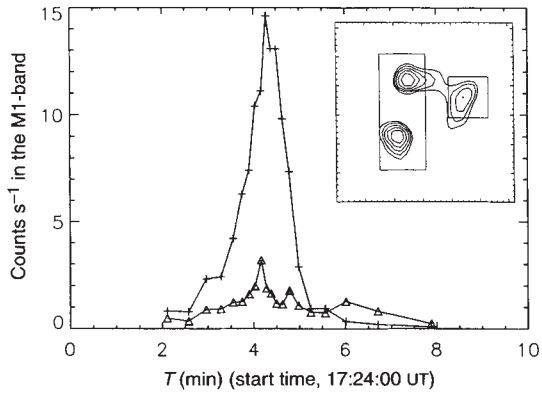

FIG. 2 Temporal behaviour of the loop-top (crosses) and double footpoint (triangles) sources in the HXT M1-band. The integrated intensities are estimated for the two boxed areas, that is, one for the loop-top source and the other for the double footpoint sources (inset). It is clear that the loop-top source varies almost coincidentally with the double footpoint sources. The integrated intensities are given in units of HXT photon counts averaged over its 64 detectors (subcollimators) whose average geometrical aperture is ~1 cm^2.

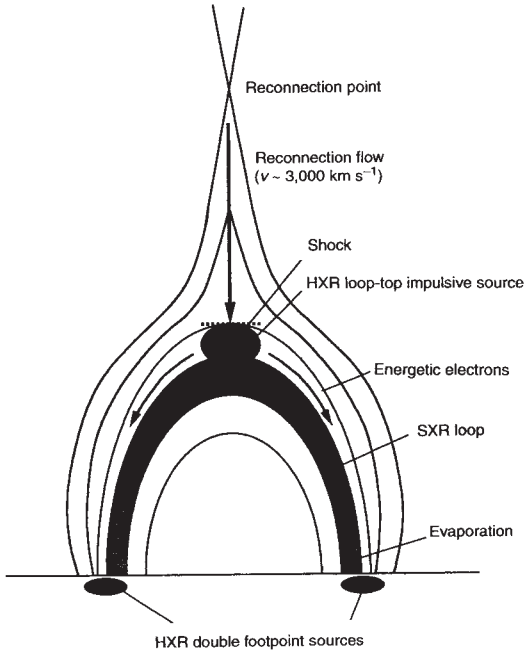

FIG. 3 The magnetic-field geometry for reconnection derived from the present observation. The important features are: elongated antiparallel magnetic fields above an arcade of closed loops; a current sheet (or neutral sheet) formation between them and reconnection of antiparallel magnetic fields. An outflow or jet from the reconnection point impinges on the underlying closed loop and forms a shock, resulting in a high-temperature ($T_e \sim 2 \times 10^8$ K) region just above the closed loop. It is also likely that electrons are accelerated in the shock and stream down along the reconnected field towards the double footpoint sources.

is formed and no strong energization occurs. The soft X-ray flaring loop may represent previously reconnected magnetic fields filled with material evaporated from the dense chromosphere. Perhaps the evaporation is caused not only by energetic electron precipitation but also by heat conduction. In any case, it is a byproduct of the primary energy release.

The observations reported here have revealed for the first time the existence of a loop-top impulsive hard X-ray source in a compact solar flare. There are other examples of this type of source in the Yohkoh data base[22]. We believe that these observations may simplify our theoretical view of solar-flare energy release. The data strongly suggest that we have identified the site of the powerful acceleration of energetic electrons common to solar flares, namely a coronal current sheet. It may now be possible for magnetic reconnection on macroscopic scales to explain compact flares as well as two-ribbon flares. Our discussion of these observations invokes shock formation resulting from the reconnection jet expected in a current-sheet configuration. This discussion was more illustrative than quantitative; it will be instructive to pursue a more thorough analysis of both Yohkoh and ground-based data on this and related flares. □

Received 12 May; accepted 19 August 1994.

1. Pallavicini, R. *Phil. Trans. R. Soc.* A**336,** 389–400 (1991).
2. Carmichael, H. in *AAS-NASA Symp. on the Physics of Solar Flares, NASA-SP 50* (ed. Hess, W. N.) 451–456 (NASA, Washington DC, 1964).
3. Sturrock, P. A. *Nature* **211,** 695–697 (1966).
4. Hirayama, T. *Sol. Phys.* **34,** 323–338 (1974).
5. Kopp, R. A. & Pneuman, G. W. *Sol. Phys.* **50,** 85–98 (1976).
6. Hayvaerts, J., Priest, E. R. & Rust, D. M. *Astrophys. J.* **216,** 123–137 (1977).
7. Tsuneta, S. *et al. Publs astr. Soc. Japan* **44,** L63–L69 (1992).
8. Tsuneta, S. in *The Magnetic and Velocity Fields of Solar Active Regions, IAU Colloq. 141* (eds Zirin, H., Ai, G. & Wang, H.) 239–248 (Astr. Soc. Pacific, San Francisco, 1993).
9. Tsuneta, S. in *X-Ray Solar Physics from Yohkoh* (eds Uchica, Y., Watanabe, T., Shibata, K. & Hudson, H. S.) 115–119 (Universal Academy Press, Tokyo, 1994).
10. Tsuneta, S. *et al. Publs astr. Soc. Japan* **44,** L211–L214 (1992).
11. Ogawara, Y. *et al. Sol. Phys.* **136,** 1–16 (1991).
12. Kosugi, T. *et al. Sol. Phys.* **136,** 17–36 (1991).
13. Tsuneta, S. *et al. Sol. Phys.* **136,** 37–67 (1991).
14. Hoyng, P. *et al. Astrophys. J.* **244,** L153–L156 (1981).
15. Duijveman, A., Hoyng, P. & Machado, M. E. *Sol. Phys.* **81,** 137–157 (1982).
16. Sakao, T. thesis, Univ. Tokyo (1994).
17. Hudson, H. S. *et al. Astrophys. J.* **422,** L25–L27 (1994).
18. Hudson, H. S. in *High-Energy Solar Phenomena—A New Era of Spacecraft Measurements AIP Conf. Proc. 294* (eds Ryan, J. M. & Vestrand, W. T.) 151–161 (AIP, New York, 1994).
19. Haisch, B., Strong, K. T. & Rodono, M. *A. Rev. Astr. Astrophys.* **29,** 275–324 (1991).
20. Brown, J. C. *Sol. Phys.* **18,** 489–502 (1971).
21. Hudson, H. S., Canfield, R. C. & Kane, S. R. *Sol. Phys.* **60,** 137–142 (1978).
22. Masuda, S. thesis, Univ. Tokyo (1994).

ACKNOWLEDGEMENTS. We thank H. Hudson for help in polishing the manuscript. The Yohkoh satellite is a Japanese national project, launched and operated by ISAS involving many domestic institutions, with multilateral international collaboration with US and UK.

A photorefractive polymer with high optical gain and diffraction efficiency near 100%

K. Meerholz*, B. L. Volodin*, Sandalphon*, B. Kippelen† & N. Peyghambarian*

* Optical Sciences Center, University of Arizona, Tucson, Arizona 85721, USA
† IPCMS, Groupe d'Optique Nonlinéaire et d'Optoélectronique, Unité Mixte CNRS-ULP-EHICS, Strasbourg, France

PHOTOREFRACTIVE materials are of considerable interest for the development of all-optical devices[1]. The photorefractive effect appears in materials that exhibit an electric-field-dependent refractive index and that are photosensitive, such that the spatial distribution of photogenerated charge carriers is modified on irradiation with light. The diffraction pattern formed by the interference of two coherent light beams within such a material generates a non-uniform internal electric field that in turn modulates the refractive index. The resulting refractive-index pattern forms a grating that can diffract light and thereby give rise to two-beam coupling, whereby one of the writing beams gains energy at the expense of the other—a property that can be exploited in photonic devices. Although the best photorefractive materials currently available are inorganic crystals such as $LiNbO_3$, there is considerable interest in the development of photorefractive polymers[2–8], owing to their structural flexibility, ease of processing and lower cost. We describe here a polymer composite with excellent photorefractive properties. We have achieved a diffraction efficiency approaching 100% and a net two-beam coupling gain of more than 200 cm^{-1}, making these polymeric materials suitable for immediate application in areas such as dynamic holographic storage and optical information processing[1].

In organic materials, the properties required for the photorefractive effect, including photosensitivity, photoconductivity and electro-optic response, are provided by different molecules. As a result, the properties can be optimized separately, unlike in inorganic photorefractive crystals such as $LiNbO_3$. Our investigations were performed on a polymer composite (see Fig. 1) based on the photoconductor poly(*N*-vinylcarbazole) (PVK). Composites using PVK were the first polymers to show efficient photorefractivity[6] and are still among the organic materials with the best performances[4,7]. Photosensitivity in the visible was provided by adding a small amount of 2,4,7-trinitro-9-fluorenone (TNF), which forms a charge-transfer complex with PVK. Crucial for the steady-state performance of a photorefractive composite is the electro-optic chromophore. The latter should possess a large dipole moment μ, a large first hyperpolarizability β, and at the same time a small absorption coefficient α at the operating wavelength. The electro-optic chromophore should be highly soluble in the composite to obtain a strong photorefractive effect. Furthermore, as will be shown below, a large aniso-